Radiation Characteristics of an Infinite Dielectric-Coated Axially Slotted Cylindrical Antenna Partly Embedded in a Ground Plane

Hassan A. Ragheb, *Senior Member, IEEE*, and Umar M. Johar

***Abstract*— The radiation characteristics of an axial slot on a dielectric-coated conducting circular cylinder embedded in a semi-circle in an infinite ground plane (GP) are examined. The boundary-value method is employed to obtain the solution with the aid of the partial orthogonality of the trigonometric functions. The resulting dual infinite series involved in the solution is then truncated to generate numerical results. The geometry considered here is important because it can be implemented on the body of any mobile communication system. Moreover the GP adds a new parameter to the slotted dielectric-coated conducting circular cylindrical antenna and can be used in beam shaping and to enhance the antenna performance.**

***Index Terms*—Electromagnetic radiation, slot antennas.**

I. Introduction

RADIATION from axial and circumferential slots on a circular conducting cylinder has been the subject of extensive investigations. For instance, the residue series and the geometrical optics representation [1], Green's function formulation [2] and the Fourier integral representation [3] have been employed for analytical treatment of different slots on a circular conducting cylinder. Also, the dielectric-coated conducting slotted circular cylinder has been examined [4], [5]. Various methods similar to these used for the circular conducting slotted antenna were employed in the two-dimensional (2-D) and three-dimensional cases to obtain different radiation characteristics of the dielectric-coated slotted cylindrical antenna [6]–[8]. In all previous work, the effect of mounting the antenna on any communication system has been ignored. The subject of this work is to present the effect of an infinite ground plane (GP) on the dielectric-coated cylindrical axial-slot antenna. The GP could be the body of an air craft, a ship, or any other mobile system. This effect could enhance the radiations characteristics in some cases. The GP can be used to support the slotted dielectric-coated conducting circular cylindrical antenna. The addition of the GP will add another parameter to the design of the antenna such that it can be used to improve the antenna performance. The problem under consideration is solved using the boundary-value method. The partial othogonality propriety used in [9] is employed here to obtain an analytical solution. The resulting solution involves a double series, which is convergent and will be truncated in the numerical calculations. Examples are introduced to show the effect of the GP and how it can be used to improve the radiation patterns.

Manuscript received June 20, 1997; revised April 27, 1998.

The authors are with the Department of Electrical Engineering, King Fahd University of Petroleum and Minerals, Dhahran 31262, Saudi Arabia.

Publisher Item Identifier S 0018-926X(98)07503-6.

II. Formulation of the TM Case

A 2-D cross section of the geometry of the problem is shown in Fig. 1. The conducting circular cylinder has a radius "a," while the dielectric coating has an outer radius "b," permittivity "ε," and permeability "μ." The GP is assumed to be perfectly conducting and the axial slot is centered at ϕ_o and has an angular angle which equals 2θ. The space surrounding the slotted cylinder is divided into two regions. Region I is outside the dielectric coating, while region II is inside the dielectric coating. The electric field in region I must have zero value at ϕ equal 0 and π. Therefore, the z component of the electric field in region I can be written in terms of the coordinate system at the center of the conducting cylinder as

$$E_z^{(\mathrm{I})} = E_o \sum_{n=1}^{\infty} A_n^{\mathrm{TM}} H_n^{(2)}(k_o r) \sin n\phi \tag{1}$$

where the time dependence $e^{j\omega t}$ is assumed and omitted throughout. k_o is the free-space wavenumber $(2\pi/\lambda)$ where λ is the wavelength. The above equation results from solving the Helmholtz wave equation in cylindrical coordinates. Similarly, the z component of the electric field in region II can be expressed as a Fourier Bessel infinite series of unknown coefficients, i.e.,

$$E_z^{(\mathrm{II})} = E_o \sum_{n=-\infty}^{\infty} \{B_n^{\mathrm{TM}} J_n(kr) + C_n^{\mathrm{TM}} Y_n(kr)\} e^{jn\phi} \tag{2}$$

where $k = k_o\sqrt{\mu_r \epsilon_r}$, and $J_n(x)$ and $Y_n(x)$ are Bessel functions of the first and second kind, respectively, of order n and argument x. The field component $H_z = 0$, while H_ϕ is equal to $(1/j\omega\mu)(\partial E_z/\partial r)$. The boundary condition of the vanishing tangential component of the electric field on the surface of conducting cylinder, except on the axial slot, is applied to obtain

$$E_o \sum_{n=-\infty}^{\infty} \{B_n^{\mathrm{TM}} J_n(ka) + C_n^{\mathrm{TM}} Y_n(ka)\} e^{jn\phi} = \begin{cases} E_z(\phi), & \phi_1 \le \phi \le \phi_2 \\ 0, & \text{otherwise} \end{cases} \tag{3}$$

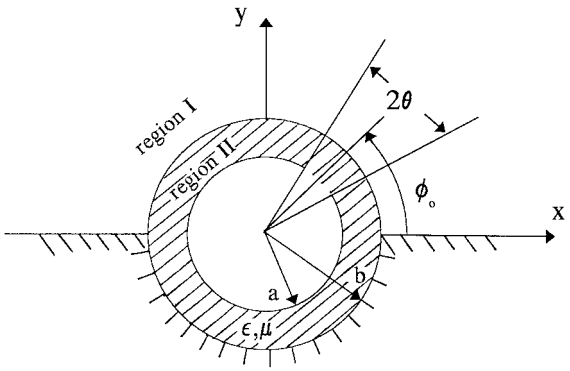

Fig. 1. Geometry of the antenna.

where $E_z(\phi)$ is the electric field on the axial-slot aperture, which is assumed to be

$$E_z(\phi) = E_o \cos\left(\frac{\pi(\phi-\phi_o)}{2\theta}\right). \tag{4}$$

Multiplying both sides of (3) by $e^{-jm\phi}$ and integrating over ϕ from 0 to 2π with some mathematical manipulations one obtains

$$B_m^{\mathrm{TM}} = \frac{1}{J_m(ka)}\left\{X_m^{\mathrm{TM}} e^{-jm\phi_o} - C_m^{\mathrm{TM}} Y_m(ka)\right\} \tag{5}$$

where

$$X_m^{\mathrm{TM}} = \frac{2E_o\theta\cos m\theta}{\pi^2 - 4\theta^2 m^2}. \tag{6}$$

The boundary conditions of the zero tangential electric field at $r = b$ and $\pi < \phi < 2\pi$ and continuous fields (i.e., E_z and H_ϕ) across the aperture $0 < \phi < \pi$ are applied to obtain (7)–(9), shown at the bottom of the page, where v_n equals one for $n = 0$ and two otherwise, and

$$\alpha_n^{\mathrm{TM}} = J_n(kb)Y_n(ka) - J_n(ka)Y_n(kb) \tag{10}$$

$$\alpha_n'^{\mathrm{TM}} = J_n'(kb)Y_n(ka) - J_n(ka)Y_n'(kb) \tag{11}$$

the primed Bessel functions in the above expressions denote their derivatives with respect to the argument. Changing $\phi \to \phi - \pi$ in (8), (8)–(10), shown at the bottom of the page, can be written as

$$\sum_{n=0}^{\infty} g_n(kb)\cos n\phi = \sum_{n=1}^{\infty} f_n(k'b)\sin n\phi. \tag{12}$$

The partial orthogonality of the sinusoid of (12) over zero to π is given by [9]

$$f_m(k'b) = \frac{4}{\pi} \sum_{\substack{n=0 \\ [(m+n)\,\mathrm{odd}]}}^{\infty} \frac{m g_n(kb)}{m^2 - n^2} \qquad m = 1, 2, 3, \cdots \tag{13}$$

employing (13) in (7)–(9) with the necessary mathematical manipulation one obtains

$$\frac{e_r X_m^{\mathrm{TM}} H_m^{(2)}(k_o b)\sin m\phi_o}{kb} - \sum_{\substack{n=0 \\ [(m+n)\,\mathrm{odd}]}}^{\infty} \frac{m}{m^2 - n^2} \cdot \frac{v_n X_n^{\mathrm{TM}} \cos n\phi_o}{J_n(ka)} \left[\gamma_{m,m}^{\mathrm{TM}} J_n(kb) + \beta_{n,m}^{\mathrm{TM}} \alpha_m^{\mathrm{TM}}\right] = \sum_{\substack{n=0 \\ [(m+n)\,\mathrm{odd}]}}^{\infty} \frac{m}{m^2 - n^2} \frac{D_n^{\mathrm{TM}}}{J_n(ka)} \left[\gamma_{m,m}^{\mathrm{TM}} \alpha_n^{\mathrm{TM}} + \gamma_{n,m}^{\mathrm{TM}} \alpha_m^{\mathrm{TM}}\right] \qquad m = 1, 2, 3 \tag{14}$$

where

$$\beta_{n,m}^{\mathrm{TM}} = J_n(kb)H_m^{(2)'}(k_o b) - e_r J_n'(kb)H_m^{(2)}(k_o b) \tag{15}$$

$$\gamma_{n,m}^{\mathrm{TM}} = \alpha_n^{\mathrm{TM}} H_m^{(2)'}(k_o b) - e_r \alpha_n'^{\mathrm{TM}} H_m^{(2)}(k_o b) \tag{16}$$

and $e_r = \sqrt{\varepsilon_r/\mu_r}$. Equation (14) can be solved numerically to obtain the constants D_n^{TM}. The infinite series involved in the solution is convergent, therefore, it will be truncated after a limited number of terms which depends on the largest argument of the Bessel function (i.e., kb). Once the values of D_n^{TM} are calculated, the coefficients A_l^{TM} can be calculated from (17), shown at the bottom of the next page.

$$\sum_{n=0}^{\infty}\left\{v_n X_n^{\mathrm{TM}}\cos n\phi_o \frac{J_n(kb)}{J_n(ka)} + D_n^{\mathrm{TM}}\frac{\alpha_n^{\mathrm{TM}}}{J_n(ka)}\right\}\cos n\phi = -\sum_{n=1}^{\infty}\left\{2X_n^{\mathrm{TM}}\sin n\phi_o \frac{J_n(kb)}{J_n(ka)} + G_n^{\mathrm{TM}}\frac{\alpha_n^{\mathrm{TM}}}{J_n(ka)}\right\}\sin n\phi, \qquad \pi < \phi < 2\pi \tag{7}$$

$$\sum_{n=0}^{\infty}\left\{v_n X_n^{\mathrm{TM}}\cos n\phi_o \frac{J_n(kb)}{J_n(ka)} + D_n^{\mathrm{TM}}\frac{\alpha_n^{\mathrm{TM}}}{J_n(ka)}\right\}\cos n\phi = \sum_{n=1}^{\infty}\left\{A_n^{\mathrm{TM}}H_n^{(2)}(k_o b) - 2X_n^{\mathrm{TM}}\sin n\phi_o \frac{J_n(kb)}{J_n(ka)} - G_n^{\mathrm{TM}}\frac{\alpha_n^{\mathrm{TM}}}{J_n(ka)}\right\}\sin n\phi, \qquad 0 < \phi < \pi \tag{8}$$

$$\sum_{n=0}^{\infty}\left\{v_n X_n^{\mathrm{TM}}\cos n\phi_o \frac{J_n'(kb)}{J_n(ka)} + D_n^{\mathrm{TM}}\frac{\alpha_n'^{\mathrm{TM}}}{J_n(ka)}\right\}\cos n\phi = \sum_{n=1}^{\infty}\left\{\sqrt{\frac{\mu_r}{\epsilon_r}}\,A_n^{\mathrm{TM}}H_n^{(2)'}(k_o b) - 2X_n^{\mathrm{TM}}\sin n\phi_o \frac{J_n'(kb)}{J_n(ka)} - G_n^{\mathrm{TM}}\frac{\alpha_n'^{\mathrm{TM}}}{J_n(ka)}\right\}\sin n\phi, \ 0 < \phi < \pi. \tag{9}$$

III. Formulation of the TE Case

For TE case, the z component of the magnetic field in region I can be represented as a summation of Hankel functions. The boundary condition of the vanishing $E_r^{(\mathrm{I})}$ at ϕ equals zero and π must be imposed. In this case the z component of the magnetic field in region I can be written as

$$H_z^{(\mathrm{I})} = \sum_{n=0}^{\infty} A_n^{\mathrm{TE}} H_n^{(2)}(k_o r)\cos n\phi. \tag{18}$$

Similarly, the z component of the magnetic field in region II can be expressed as a Fourier Bessel infinite series of unknown coefficients, i.e.,

$$H_z^{(\mathrm{II})} = \sum_{n=-\infty}^{\infty} \left\{B_n^{\mathrm{TE}} J_n(kr) + C_n^{\mathrm{TE}} Y_n(kr)\right\} e^{jn\phi}. \tag{19}$$

The field component $E_z = 0$, while E_ϕ is equal to $(j/\omega\varepsilon)(\partial H_z/\partial r)$, which results in

$$E_\phi^{(\mathrm{II})} = \sum_{n=-\infty}^{\infty} j\eta\left\{B_n^{TE} J_n'(kr) + C_n^{TE} Y_n'(kr)\right\} e^{jn\phi} \tag{20}$$

where $\eta = \sqrt{\mu/\varepsilon}$. The boundary condition of vanishing tangential component of electric field on the surface of conducting cylinder except on the axial slot is applied to obtain

$$j\eta \sum_{n=-\infty}^{\infty} \{B_n J_n'(ka) + C_n Y_n'(ka)\} e^{jn\phi} = \begin{cases} E_o & \phi_1 \le \phi \le \phi_2 \\ 0, & \text{otherwise} \end{cases} \tag{21}$$

where E_o is the electric field on the axial slot aperture.

Following the same steps used for TM case one obtains (22), shown at the bottom of the next page, where

$$X_m^{\mathrm{TE}} = E_o \frac{\sin m\theta}{\pi m} \tag{23}$$

$$\alpha_n^{\mathrm{TE}} = J_n(kb) - \frac{J_n'(ka)}{Y_n'(ka)} Y_n(kb) \tag{24}$$

$$\alpha_n'^{\mathrm{TE}} = J_n'(kb) - \frac{J_n'(ka)}{Y_n'(ka)} Y_n'(kb) \tag{25}$$

$$\beta_{n,m}^{\mathrm{TE}} = H_m^{(2)}(k_o b)\frac{Y_n'(kb)}{Y_n'(ka)} - \frac{1}{e_r} H_m^{(2)'}(k_o b)\frac{Y_n(kb)}{Y_n'(ka)} \tag{26}$$

$$\gamma_{n,m}^{\mathrm{TE}} = \alpha_m' H_n^{(2)}(k_o b) - \frac{1}{e_r}\alpha_m H_n^{(2)'}(k_o b). \tag{27}$$

Equation (22) can be solved numerically to obtain the constants D_n^{TE}. Once the values of D_n^{TE} are calculated the coefficients A_l^{TE} can be calculated from (28), shown at the bottom of the next page.

IV. Radiation Pattern and Slot Conductance

The far-zone radiation pattern for the electric field of the TM case and the magnetic field of the TE case can be calculated using the asymptotic expansions of $H_m^{(2)}$ [10], i.e.,

$$E_z^{(\mathrm{I})} = \sqrt{\frac{2}{\pi kr}}\, e^{-jkr} e^{j\pi/4} P_{\mathrm{TM}}(\phi),$$
$$H_z^{(\mathrm{I})} = \sqrt{\frac{2}{\pi kr}}\, e^{-jkr} e^{j\pi/4} P_{\mathrm{TE}}(\phi) \tag{29}$$

where

$$P_{\substack{\mathrm{TM}\\ \mathrm{TE}}}(\phi) = \sum_{m=0}^{\infty} j^m \begin{matrix} A_m^{\mathrm{TM}} \sin m\phi \\ A_m^{\mathrm{TE}} \cos m\phi \end{matrix}. \tag{30}$$

The antenna gain and the aperture conductance are quantities of interest. Following the definitions of Richmond [11], one can obtain the antenna gain as

$$G(\phi) = \frac{2|P_i(\phi)|^2}{\sum_{m=0}^{\infty} |A_m^i|^2}, \qquad \text{where } i \text{ denotes TM or TE} \tag{31}$$

and the aperture conductance is

$$G_{ai}/\lambda = \left\{ \begin{matrix} \dfrac{1}{120\pi^2} \dfrac{\sum_0^{\infty} |A_m^{\mathrm{TM}}|^2}{|E_{oi}|^2} & \text{TM case} \\ \dfrac{30}{a^2\theta^2 E_{oi}^2} \sum_0^{\infty} |A_m^{\mathrm{TE}}|^2 & \text{TE case} \end{matrix} \right\}. \tag{32}$$

V. Results and Discussion

The accuracy of our numerical computations must be checked first. For this purpose, the special case of an axial slot on a conducting circular cylinder embedded in a GP will be introduced. The integral equation formulation (IEF) along with the method of moments are used to obtain results corresponding to the special case. Fig. 2 illustrates the far-field patterns for both the TM and the TE cases corresponding to IEF and our solution of an infinite GP (IGP). As one can see for the TM case the agreement is excellent at most values of ϕ except near the GP where some deviation is noticed.

$$A_l^{\mathrm{TM}} = \frac{1}{\gamma_{l,l}^{\mathrm{TM}}} \left\{ \frac{4e_r X_l^{\mathrm{TM}} \sin l\phi_o}{\pi kb} - \frac{4}{\pi} \sum_{\substack{n=0 \\ [(l+n)\,\mathrm{odd}]}}^{\infty} \frac{l}{l^2-n^2} \frac{e_r v_n X_n^{\mathrm{TM}} \cos n\phi_o}{J_n(ka)} \left[\alpha_l'^{\mathrm{TM}} J_n(kb) - J_n'(kb)\alpha_l^{\mathrm{TM}}\right] - \frac{4}{\pi} \cdot \sum_{\substack{n=0 \\ [(l+n)\,\mathrm{odd}]}}^{\infty} \frac{l}{l^2-n^2} \frac{e_r D_n^{\mathrm{TM}}}{J_n(ka)} \left[\alpha_l'^{\mathrm{TM}} \alpha_n^{\mathrm{TM}} - \alpha_n'^{\mathrm{TM}} \alpha_l^{\mathrm{TM}}\right] \right\}, \qquad l = 1, 2, 3, \cdots \tag{17}$$

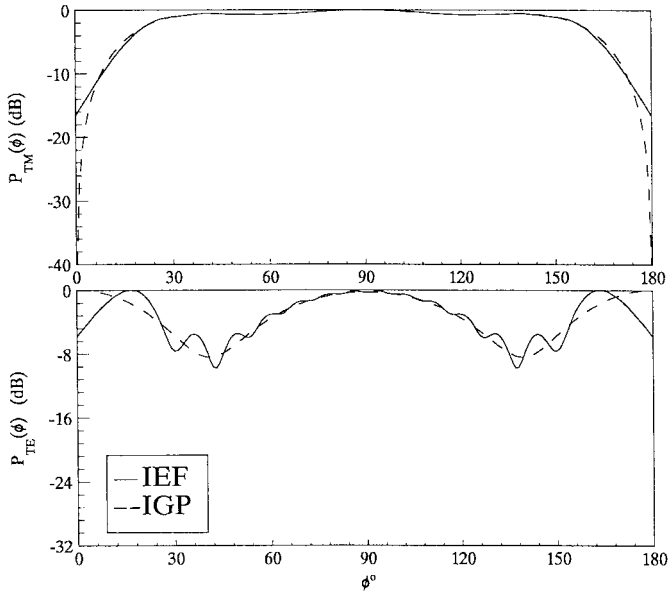

Fig. 2. Far-field pattern of an axial slot on a conducting circular cylinder embedded in a GP ($a = 0.3\lambda$, $b = 0.3\lambda$, $2\theta = 10^\circ$, $\phi_o = 90^\circ$, $\varepsilon_r = 1$, and $\mu_r = 1$).

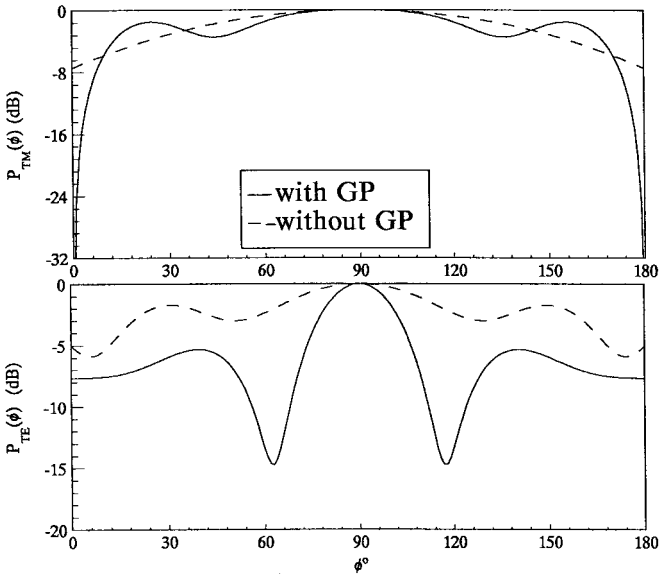

Fig. 3. Far-field pattern of an axial slot on a dielectric-coated conducting circular cylinder embedded in a GP ($a = 0.51\lambda$, $b = 0.63\lambda$, $2\theta = 10^\circ$, $\phi_o = 90^\circ$, $\varepsilon_r = 3.1$ and $\mu_r = 1$).

This is due to the truncation of the GP in our numerical calculation. For the TE case agreement is good, however, the field produced using the numerical method oscillates around the exact value, again due to the truncation of the GP in the numerical simulation. It should be mentioned here that the truncation of the infinite series (14) and (22) for producing numerical results is based on convergence criteria built in our program. Table I shows the number of terms after which truncation takes place for Figs. 2–8.

In order to present the effect of the GP on the axially slotted dielectric-coated cylindrical antenna, two groups of examples are presented. In all examples, the characteristics of the axial slot on the dielectric-coated circular cylinder are calculated with the presence of the GP and without it to study its effect. Results corresponding to cases without a GP are taken from previous work published in [12]. In the first group, the geometrical parameters are selected to produce either a narrow main beam pattern or a split main beam pattern, near the GP for the TE case. Patterns corresponding to the first example in this group are shown in Fig. 3. As one can see, the pattern produced with the existence of the GP is more directive for the TE case than the pattern without the GP. For the TM case, both patterns are almost the same except that the GP directs the pattern in the upper half-space. With a proper choice of the dielectric thickness and the same geometrical parameters

$$\frac{X_m^{\mathrm{TE}} H_m^{(2)'}(k_o b)\cos m\phi_o}{e_r Y_m'(ka)kb} - \sum_{\substack{n=1 \\ [(m+n)\,\mathrm{odd}]}}^{\infty} \frac{n}{n^2-m^2}\, 2jX_n^{\mathrm{TE}} \sin n\phi_o \left[\gamma_{m,m}^{\mathrm{TE}} \frac{Y_n'(kb)}{Y_n'(ka)} + \beta_{m,n}^{\mathrm{TE}} \alpha_m'^{\mathrm{TE}}\right]$$
$$= \sum_{\substack{n=1 \\ [(m+n)\,\mathrm{odd}]}}^{\infty} \frac{n}{n^2-m^2}\, \eta D_n^{\mathrm{TE}} \left[\gamma_{m,m}^{\mathrm{TE}} \alpha_n'^{\mathrm{TE}} + \gamma_{m,n}^{\mathrm{TE}} \alpha_m'^{\mathrm{TE}}\right], \qquad m = 0, 1, 2 \tag{22}$$

$$A_l^{\mathrm{TE}} = \frac{j}{\eta \gamma_{l,l}^{\mathrm{TE}}} \left\{ \frac{-2\nu_l X_l^{\mathrm{TE}} \cos l\phi_o}{\pi kb Y_l'(ka)} + \frac{2\nu_l}{\pi} \sum_{\substack{n=1 \\ [(l+n)\mathrm{odd}]}}^{\infty} \frac{n}{n^2-l^2} 2jX_n^{\mathrm{TE}} \sin n\phi_o \left[\alpha_l^{\mathrm{TE}} \frac{Y_n'(kb)}{Y_n'(ka)} - \alpha_l' \frac{Y_n(kb)}{Y_n'(ka)}\right] \right.$$
$$\left. + \frac{2\nu_l}{\pi} \sum_{\substack{n=1 \\ [(l+n)\mathrm{odd}]}}^{\infty} \frac{n}{n^2-l^2} \eta D_n^{\mathrm{TE}} [\alpha_n'^{\mathrm{TE}} \alpha_l^{\mathrm{TE}} - \alpha_l'^{\mathrm{TE}} \alpha_n^{\mathrm{TE}}] \right\}, \qquad l = 0, 1, 2, \cdots \tag{28}$$

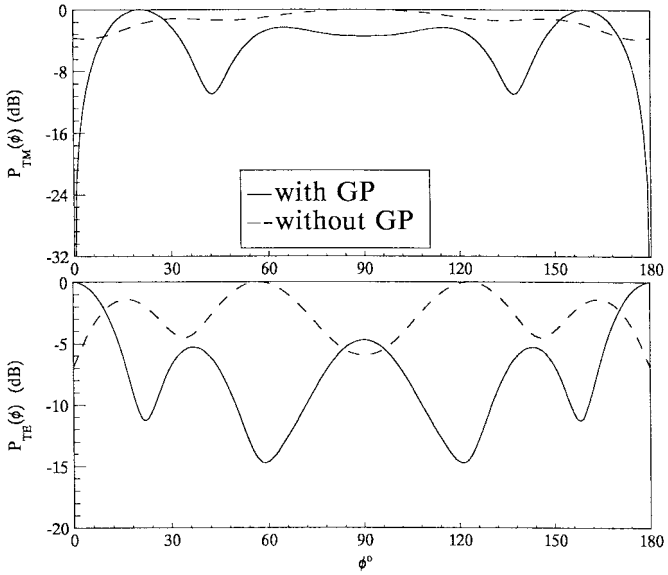

Fig. 4. Far-field pattern of an axial slot on a dielectric-coated conducting circular cylinder embedded in a GP ($a = 0.51\lambda$, $ab = 0.70\lambda$, $2\theta = 10^\circ$, $\phi_o = 90^\circ$, $\varepsilon_r = 3.1$, and $\mu_r = 1$).

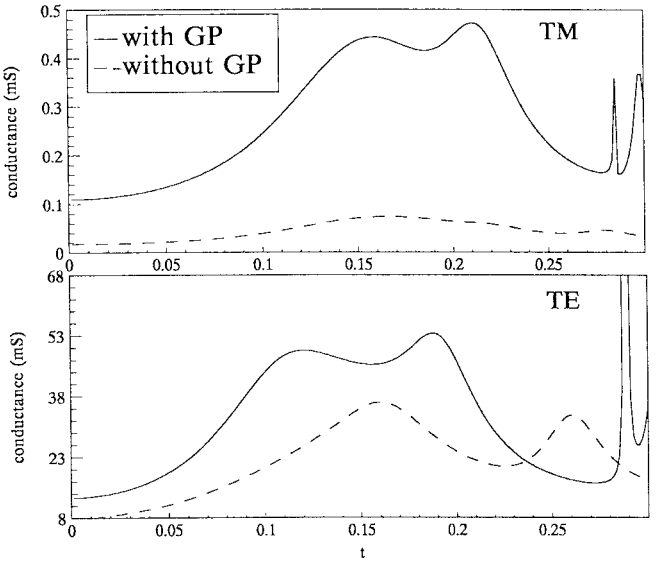

Fig. 6. Aperture conductance of an axial slot on a dielectric-coated conducting circular cylinder embedded in a GP versus coating thickness t ($a = 0.51\lambda$, $2\theta = 10^\circ$, $\phi_o = 90^\circ$, $\varepsilon_r = 3.1$, and $\mu_r = 1$).

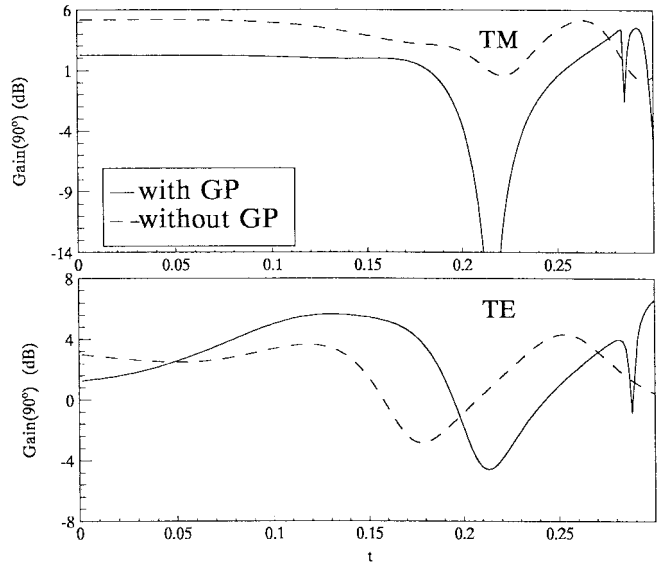

Fig. 5. Gain at 90° of an axial slot on a dielectric-coated conducting circular cylinder embedded in a GP versus coating thickness t ($a = 0.51\lambda$, $2\theta = 10^\circ$, $\phi_o = 90^\circ$, $\varepsilon_r = 3.1$, and $\mu_r = 1$).

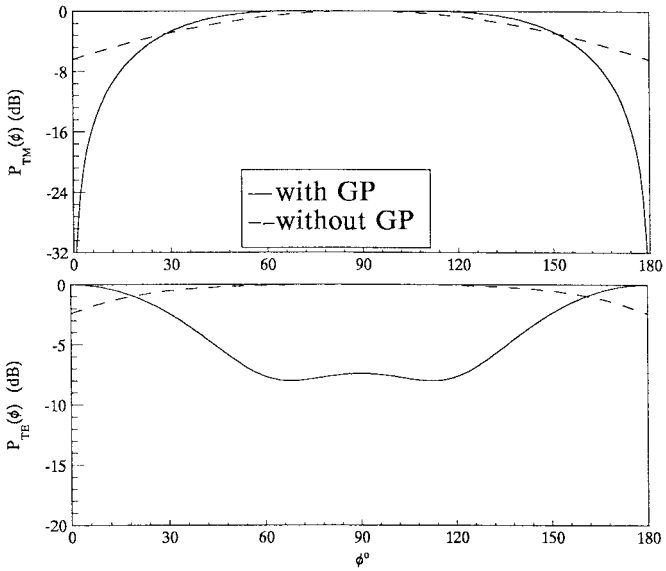

Fig. 7. Far-field pattern of an axial slot on a dielectric-coated conducting circular cylinder embedded in a GP ($a = 0.16\lambda$, $b = 0.20\lambda$, $2\theta = 10^\circ$, $\phi_o = 90^\circ$, $\varepsilon_r = 2.6$, and $\mu_r = 1$).

(as in the first example) one can obtain a main beam split near the GP for the TE case as shown in Fig. 4. These two examples show that the GP is adding a new parameter that can be used for pattern shaping. In Fig. 5, the gain at the slot center (90°) for different values of the dielectric thickness ($t = b - a$) is plotted for both TM and TE cases. One can see that for the TM case the average values of the gain with the GP are less than their corresponding values without the GP. But for the TE case, the gain is higher with a GP than without a GP at most values of the dielectric thickness. The aperture conductance is also calculated for different values of the dielectric thickness as shown in Fig. 6. It is found that the aperture conductance with the GP is higher than without the GP for both cases.

In the second group of examples our design criteria is to produce either a flat pattern in a wide space or a two beam pattern for the TM case. In the first example of this group the geometrical parameters are selected to produce a TM flat pattern. Fig. 7 shows radiation patterns for both TM an TE cases for this example. As one can see, for the TM case a flat pattern in the range of ϕ between 30 and 150° is obtained. The pattern corresponding to the TE case of this example has main beam split near the GP as shown in Fig. 7. The same geometrical parameters are used except that the dielectric thickness is changed to produce a TM two-beam pattern. Fig. 8 illustrates the resulting patterns in this case. As one can see, a two-beam pattern is obtained for the TM case, while the

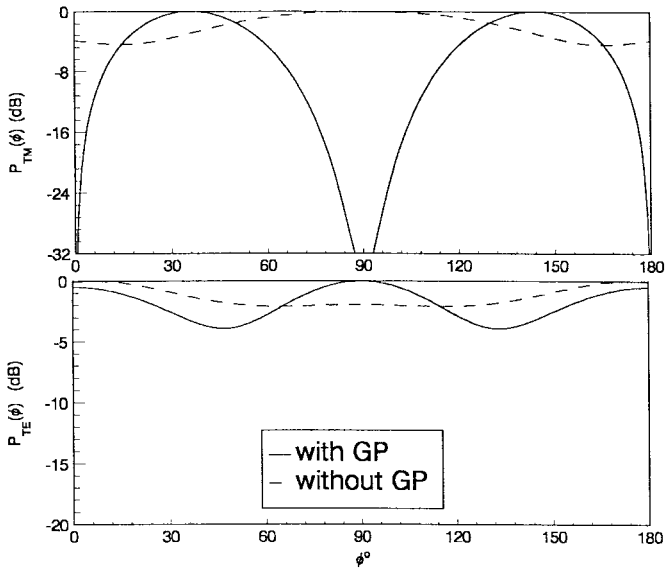

Fig. 8. Far-field pattern of an axial slot on a dielectric-coated conducting circular cylinder embedded in a GP ($a = 0.16\lambda$, $b = 0.40\lambda$, $2\theta = 10^\circ$, $\phi_o = 90^\circ$, $\varepsilon_r = 2.6$, and $\mu_r = 1$).

TABLE I
TRUNCATION NUMBER OF THE INFINITE SERIES (14) AND (22) FOR FIGS. 2–8

	Number of terms used	
Figure #	TM	TE
2	10	10
3	12	14
4	12	14
5	12-14	14-16
6	12-14	14-16
7	8	10
8	10	10

pattern corresponding to the TE case has slight change when it is compared with its equivalent without a GP.

VI. CONCLUSION

The effect of a GP on dielectric-coated axially slotted conducting circular cylindrical antennas is presented. It is demonstrated that the GP can be used to improve the antenna performance. Analytical solutions based on the boundary value method are obtained. The GP can be used to mount the antenna and could represent part of a ship, an aircraft, or any other communication system. Meanwhile, with proper design, its effect can be tuned to enhance the antenna characteristics.

ACKNOWLEDGMENT

The authors would like to thank KFUPM for providing all the facilities required to perform this research.

REFERENCES

[1] S. Sensiper, "Cylindrical radio waves," *IRE Trans. Antennas Propagat.*, vol. AP-5, pp. 56–70, Jan. 1957.
[2] H. Papas, "Radiation from a transverse slot in an infinite cylinder," *J. Math. Phys.*, vol. XXVIII, pp. 227–236, 1949.
[3] S. Silver and W. K. Saunders, "The radiation from a transverse rectangular slot in a circular cylinder," *J. Appl. Phys.*, vol. 21, pp. 153–158, Feb. 1950.
[4] R. A. Hurd, "Radiation pattern of a dielectric-coated axially-slotted cylinder," *Canadian J. Phys.*, vol. 34, pp. 638–642, 1956.
[5] J. R. Wait and W. Mientka, "Slotted-cylinder antenna with a dielectric coating," *J. Res. Nat. Bureau Standards*, vol. 58, pp. 287–296, June 1957.
[6] L. Shafai, "Radiation from an axial slot antenna coated with a homogeneous material," *Canadian J. Phys.*, vol. 50, pp. 3072–3077, 1972.
[7] C. M. Knop, "External admittance of an axial slot on a dielectric-coated metal cylinder," *Radio Sci.*, vol. 3, pp. 803–817, Aug. 1968.
[8] W. Crosswell, G. Westrick, and C. Knop, "Computations of the aperture admittance of an axial slot on a dielectric-coated cylinder," *IEEE Trans. Antennas Propagat.*, vol. AP-20, pp. 89–92, 1972.
[9] M. Hinders and A. Yaghjian, "Dual-series solution to scattering from a semicircular channel in a ground plane," *IEEE Microwave Guided Wave Lett.*, vol. 1, pp. 239–242, Sept. 1991.
[10] J. A. Stratton, *Electromagnetic Theory*. New York: McGraw-Hill, 1941.
[11] J. Richmond, "Axial slot antenna on dielectric-coated elliptic cylinder," *IEEE Trans. Antennas Propagat.*, vol. 37, pp. 1235–1241, Oct. 1989.
[12] H. Ragheb and E. Hassan, "Radiation characteristics of slots on a conducting circular cylinder covered by eccentric dielectric cylinder," *Proc. Inst. Elect. Eng., Microwave Antennas Propagat.*, vol. 142, pp. 168–172, 1995.

Hassan A. Ragheb (M'89–SM'94) was born in Port Said, Egypt, in 1953. He received the B.Sc. degree in electrical engineering from Cairo University, Egypt, in 1977, and the M.Sc. and Ph.D. degrees in electrical engineering from the University of Manitoba, Winnipeg, Canada, in 1984 and 1987, respectively.

From 1987 to 1989, he was a Research Assistant in the Department of Electrical Engineering, University of Manitoba. In 1989, he joined the Department of Electrical Engineering at the King Fahd University of Petroleum and Minerals, where he is now an Associate Professor of electrical engineering. From 1995 to 1996, while on sabbatical, he was with the Electrial and Computer Engineering Department of the University of Manitoba. His research interests include electromagnetic scattering by multiple and coated objects, microstrip antennas, phases arrays, and slot antennas.

Umar M. Johar was born in Asmara, Eritrea, on February 3, 1967. He received the B.Sc. and M.Sc. degrees in electrical engineering from King Fahd University of Petroleum and Minerals, Dhahran, Saudi Arabia, in 1990 and 1993, respectively.

He worked as a Research Assistant in the Department of Electrical Engineering at King Fahd University of Petroleum and Minerals from November 1990 to January 1993. In February 1993, he joined the same department as a Lecturer. His current research interests include microwaves, numerical analysis of electromagnetic fields, and integrated optics.